# Sterically Hindered, Saddle-Shaped Complexes of Palladium(II) and Platinum(II) and Their Reaction with Iodine[1a]

**Alan J. Jircitano,[1b] Mark D. Timken,[1b] Kristin Bowman Mertes,*[1b] and John R. Ferraro[1c]**

*Contribution from the Department of Chemistry, University of Kansas, Lawrence, Kansas 66045, and the Chemistry Division, Argonne National Laboratory, Argonne, Illinois 60439.* *Received April 27, 1979*

**Abstract:** The synthesis and characterization of $I_2$ reaction products of palladium(II) and platinum(II) with the tetraaza macrocycle tetrabenzo[*b,f,j,n*][1,5,9,13]tetraazacyclohexadecine (TAAB) from $[M(TAAB)][BF_4]_2$ are described. X-ray structural results for $[Pd(TAAB)][BF_4]_2$ show the complex to crystallize in the monoclinic space group $P2_1/c$ with unit cell dimensions $a$ = 16.927 (6) Å, $b$ = 11.757 (7) Å, $c$ = 15.559 (4) Å, and $\beta$ = 118.87 (2)°. The immediate coordination sphere of the palladium consists of the four nitrogens situated on a saddle-shaped surface with the palladium located essentially in the center. The ligand system is decidedly saddle shaped, with the benzo groups forming cavities 2.70 Å deep above and below the $PdN_4$ surface. In the presence of $I_2$ these complexes react to form a complex with the stoichiometry $[M(TAAB)][I_3]_{2.7}$. The presence of $I_3^-$ and absence of $I_2$ were confirmed by both far-infrared and Raman spectroscopy. Mid-infrared and EPR evidence substantiates that ligand oxidation has not occurred. Electrical conductivity measurements using dc two-probe techniques indicate an unusual pressure dependence, whereby up to a 1000-fold increase in conductivity at up to 10 kbar pressure is noted. Single-crystal conductivity measurements for $[Pt(TAAB)][I_3]_{2.7}$ indicate conductivities on the order of the partially oxidized bisdioximates ($10^{-4}$ $\Omega^{-1}$ cm$^{-1}$) while the palladium analogue is considerably less ($10^{-7}$ $\Omega^{-1}$ cm$^{-1}$).

## Introduction

The quest for materials with unusual semiconducting and conducting properties has provided impetus for research in the area of "linear chain" or "pseudo-one-dimensional" compounds. These are substances which display distinct anisotropies in the crystalline state in certain intensive physical properties. Optical, electrical, and/or magnetic behavior, for example, can be affected by virtue of the manner in which the molecules are aligned with respect to each other. Inorganic transition metal systems have been studied extensively.[2a] Traditionally, the synthesis of highly conducting planar metal complexes has involved (1) the use of $d^8$ metals, noted for their preference for square-planar geometries, (2) maximizing metal orbital interactions by employing larger metals of the second and third transition series to benefit from greater d orbital spatial extension, (3) nonbulky ligand systems to minimize intermolecular repulsions, and (4) oxidation (often with $I_2$ or $Br_2$) to create a partially filled band, a prerequisite for metallic conduction according to band theory. The extensively studied tetracyanoplatinate systems exemplify the aforementioned criteria.[2a]

More recently investigations have involved pseudomacrocyclic and macrocyclic ligand systems such as the bisdioximates,[2b,3-7] phthalocyanines,[8,9] and tetrabenzporphyrins.[9,10] Various bisdioximates of nickel(II) and palladium(II) have been shown to undergo partial oxidation in the presence of $I_2$ and $Br_2$ to yield compounds which exhibit semiconductor behavior with conductivities orders of magnitude greater than the unoxidized forms as well as metal-metal distances which are decreased by approximately 0.3 Å.[3,5] Oxidation results in removal of electrons from either a ligand-centered[11] or a metal $d_{z^2}$-like orbital[5,6] indicating the importance of both ligand- and metal-centered intermolecular interactions. Transition-metal complexes of phthalocyanines and tetrabenzporphyrins also have been reported to form highly conducting derivatives upon $I_2$ oxidation.[8-10] $(CuPc)I_{1.71}$ (Pc = phthalocyanine), for example, shows a room temperature conductivity of 4.2 $\Omega^{-1}$ cm$^{-1}$. ESR data indicates that ligand-centered interactions are mainly responsible for the conductivity behavior of these complexes.[10] Both the phthalocyanines and tetrabenzporphyrins are highly planar in contrast to the bisdioximates, which usually deviate somewhat from planarity, especially bis(diphenylglyoxime) derivatives, where the phenyl groups are rotated with respect to the $MN_4$ plane.[5]

Highly nonplanar molecules have not, in general, been investigated owing to steric influences which tend to hamper close molecular approach and hence increased intermolecular interaction. Herein are described the synthesis and characterization of the product of $I_2$ and sterically hindered saddle-shaped transition-metal complexes of palladium(II) and platinum(II) with a tetraaza macrocyclic ligand, tetrabenzo[*b,f,j,n*][1,5,9,13]tetraazacyclohexadecine (TAAB). The neutral ligand lacks two electrons for an aromatic, planar configuration. Attempts at isolating stable, planar reduction products with palladium and platinum and the ligand TAAB in order to create a desirable situation for minimizing steric repulsions were unsuccessful, however. Because of the success with ligand oxidation in the phthalocyanines and tetrabenzporphyrins,[8-10] a similar route was used for the TAAB complexes. Preliminary results on the palladium reaction product showed unusually large pressure effects on solid-state conductivity measurements.[12] The synthesis and further characterization of both the palladium and platinum products which can be formulated as $[M(TAAB)][I_3]_{2.7}$ are reported below.

## Experimental Section

**Physical Measurements.** Infrared, far-infrared, and Raman measurements were made as reported previously.[12] Pressure dependence measurements of mid-infrared spectra were made by modifying the spectrophotometer with a 4:1 beam condenser[13] and using a diamond-anvil pressure cell (DAC) calibrated by monitoring phase transitions occurring at known pressures for several solids.[14]

Both pressed-powder and single-crystal conductivities were measured. Pressure dependencies of the pressed powder conductivities were monitored using a two-probe method designed for use with the DAC.[15] A Fluke 8800A digital multimeter was employed for resistance measurements below 20 MΩ and a Keithley 610C electrometer was used for higher resistances. Single-crystal conductivities were measured at ambient temperature using a four-probe dc technique with a Hewlett-Packard power supply and a Keithley 610C electrometer.

0002-7863/79/1501-7661$01.00/0 

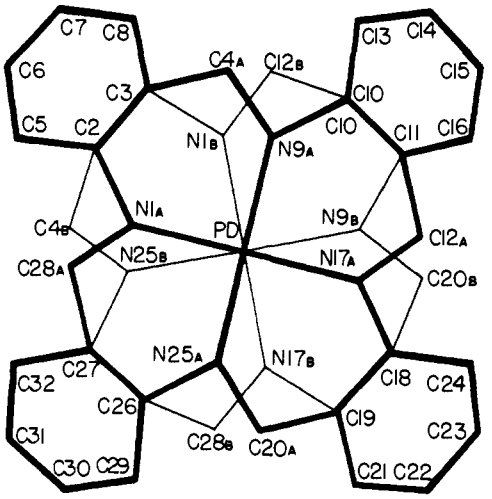


**Figure 1.** Numbering scheme and pictorial representation of the disorder in the cation $Pd(TAAB)^{2+}$.

Both EPR and the Faraday method were employed for magnetic investigations. A Varian V4502 X-band spectrometer equipped with a 6-in. magnet was used for EPR measurements. Peroxylamine disulfonate was used as a standard and taken to have a $g$ value of 2.005 50 with a hyperfine separation between the low field and center line of the $^{14}N$ three-line hyperfine pattern of 13.00 G.[16]

The X-ray photoelectron spectroscopic data was obtained using a McPherson ESCA 36 spectrometer with multichannel detection and Mg K$\alpha$ radiation. The samples were prepared using crystals which were ground and pressed into stainless steel fritted plates. The spectrometer was pumped by a turboelectric pump to a residual pressure of $4 \times 10^{-7}$ Torr, and the sample region was differentially pumped by a standard helium cryopump to a pressure at least an order of magnitude lower. Data were handled by subtracting $K\alpha_{3,4}$ satellites and smoothing using 11 points at a time. Carbon was used as a reference line at 284.8 eV.

**Synthesis.** All solvents and chemicals were reagent grade. $[M(TAAB)][BF_4]_2$ (M = Pd, Pt) were synthesized as described previously.[17] $[M(TAAB)][I_3]_{2.7}$ was synthesized by dissolving 0.5 mmol of the corresponding $BF_4$ salt in 100 mL of $CH_3CN$ and adding 2.2 mmol of $I_2$ in 80 mL of $CH_2Cl_2$. Upon slow evaporation highly lustrous, dark, metallic-appearing crystals were obtained. Analyses, shown in Table I, were performed by Micro-Tech Laboratories, Skokie, Ill.

**Structure Determination and Refinement.** Crystals of $[Pd(TAAB)][BF_4]_2$ suitable for X-ray analysis were obtained from slow evaporation of an acetonitrile solution of the complex. A crystal was chosen and mounted for preliminary precession photographs which were indicative of monoclinic symmetry with systematic absences $h0l$, $l \neq 2n$, and $0k0$, $k \neq 2n$, unequivocally a characteristic of the space group $P2_1/c$. A small, uniform rhombohedral crystal ($0.35 \times 0.35 \times 0.30$ mm) was then mounted in a random orientation for data collection, which was accomplished using a Syntex $P2_1$ automatic diffractometer equipped with a scintillation counter and graphite monochromator. Accurate centering of 15 reflections well distributed in reciprocal space resulted in unit cell dimensions $a$ = 16.927 (6) Å, $b$ = 11.757 (7) Å $c$ = 15.559 (4) Å, $\beta$ = 118.87 (2)°, and $V$ = 2712 (2) Å$^3$.[18] The density, measured to be 1.69 (1) g cm$^{-3}$ by flotation in $CH_3I$–$CCl_4$, is in agreement with the calculated density of 1.694 g cm$^{-3}$ for $Z$ = 4. The data were collected and treated as described previously.[19] Three reflections (1,1,1; −1,−1,2; 2,2,−3) chosen as standards and measured every 97 reflections showed a deviation of 2.48% during data collection for which no correction was made. A total of 7957 independent reflections were collected for which $I \geq 3\sigma(I)$ of 5959, these being used in subsequent data refinement. An absorption correction was not applied owing to the small uniform size of the crystal and the small linear absorption coefficient of 7.60 cm$^{-1}$. The structure was solved by the heavy-atom method[20] and refined by full-matrix least-squares techniques during which the function $\Sigma w(|F_o| - |F_c|)^2$ was minimized. Weights were taken as $1/\sigma_{F^2} = 4LpI/\sigma_{I^2}$. The palladium was located from a Patterson map at 0.298, 0.20, 0.84. The remainder of the nonhydrogen atoms were located from a subsequent Fourier map. The scattering factor tables for palladium were obtained from Thomas and Umeda,[21] for carbon, nitrogen, and oxygen from Cromer and Mann,[22] and for hydrogen and anomalous factors for palladium from Ibers.[23]

**Table I.** Analytical Data for $[M(TAAB)][I_3]_{2.7}$

| complex | % C | % H | % N | % I | |
|---|---|---|---|---|---|
| $[Pd(TAAB)][I_3]_{2.7}$ | 21.92 | 1.31 | 3.65 | 66.18 | calcd |
| | 21.82 | 1.31 | 3.66 | 66.23 | found |
| $[Pt(TAAB)][I_3]_{2.7}$ | 20.72 | 1.24 | 3.45 | 62.56 | calcd |
| | 20.89 | 1.26 | 3.53 | 62.76 | found |

During initial refinement it was observed that the thermal parameters for several groups of atoms were unusually large. In particular this included (1) the four C=N groups belonging to the macrocycle, (2) one entire $BF_4^-$, and (3) the F's associated with a second $BF_4^-$. Analogous to the $Ni(TAAB)^{2+}$ structures the disorder within the complex cation can best be described by considering pseudo-mirror planes to pass midway through opposite benzo rings, hence reflecting each C=N through the mirror. As a result, eight C=N positions are generated from the four C=N moieties while the benzo groups remain ordered. The latter thus seemingly dominates the spatial requirements for the complex, allowing for the dual orientation of the C=N linkages. Each model was assigned an occupancy of 0.5 and subsequent refinement resulted in a final value of 0.58 for what shall henceforth be designated model A and 0.42 for model B. Figure 1 gives a pictorial representation of the disorder. The numbering scheme for a given atom of model B is obtained by reflection of the analogous atom in model A through the pseudomirror of the benzo group with which the C=N group is associated.

The $BF_4^-$ anions were not altogether amenable to various models. One $BF_4^-$ was adequately explained by including a second orientation for the four fluorines, readily apparent in a difference Fourier. The other $BF_4^-$ had an unusually large thermal parameter for the boron. A third location for $BF_4^-$ was searched for unsuccessfully. Finally a model which incorporated two $F_4$ orientations was found to be the most agreeable. The fluorine occupancies were assigned on the basis of electron density and no correlation was found with the disordered C=N moieties.

The structure was refined to isotropic convergence, at which time all of the ordered atoms within the cation were assigned anisotropic temperature factors. A difference Fourier at this point enabled assignment of hydrogens associated with the benzo groups. The hydrogens were assigned thermal parameters of $n + 1$, $n$ being the isotropic temperature factor of the atom to which a given hydrogen is bonded. Hydrogens were included as fixed atom contributions in subsequent refinement. Because of the large number of data an abbreviated set of 5910 reflections with $\sin\theta \leq 0.70$ was used for block matrix least-squares refinement to a final $R_1 = 0.060$ and $R_2 = 0.081$ where $R_1 = \Sigma||F_o| - |F_c||/\Sigma|F_o|$ and $R_2 = (\Sigma w(|F_o| - |F_c|)^2/\Sigma w|F_o|^2)^{1/2}$.

Table II, the observed and calculated structure factors, is available as supplementary material. The final positional and thermal parameters are listed in Table III. Tables IV and V contain hydrogen atom positions and interatomic bond lengths, respectively.

## Results and Discussion

**Crystal and Molecular Structure of $[Pd(TAAB)][BF_4]_2$.** The geometry of the cation is essentially $S_4$, presenting a distinctly nonplanar, saddle-shaped appearance as seen in the overhead stereoview and in-plane perspective view in Figures 2 and 3, respectively. The $BF_4$'s are located in channels formed by parallel benzo groups of adjacent molecules as seen in the packing diagram in Figure 4. Bond lengths are reported in Table VI and angles in Table VII. The immediate coordination sphere of the palladium consists of the four nitrogens situated on a saddle-shaped surface with the palladium located essentially in the center as shown by the mean plane calculations in Table VIII. Model B shows somewhat less distortion from planarity with an average displacement of 0.158 Å for the nitrogens compared with 0.187 Å for model A. Opposing benzo groups form cavities 2.70 Å deep about the palladium. A weak axial interaction of the palladium is observed with one of the

**Table III.** Final Positional and Thermal Parameters for Nonhydrogen Atoms in $[Pd(TAAB)][BF_4]_2$[a]

| | $x$ | $y$ | $z$ | $\beta_{11}$ or $B$ | $\beta_{22}$ | $\beta_{33}$ | $\beta_{12}$ | $\beta_{13}$ | $\beta_{23}$ |
|---|---|---|---|---|---|---|---|---|---|
| Pd | 0.292 82(2) | 0.203 92(3) | 0.840 63(3) | 0.002 98(1) | 0.005 82(2) | 0.004 05(2) | 0.000 11(2) | 0.001 78(1) | −0.000 13(2) |
| N1A | 0.2079(5) | 0.0681(6) | 0.7992(5) | 3.09(11) | | | | | |
| N1B | 0.3305(6) | 0.0648(8) | 0.7968(7) | 3.20(16) | | | | | |
| C2 | 0.1894(5) | 0.0004(4) | 0.7142(4) | 0.0080(4) | 0.0045(3) | 0.0040(3) | 0.0018(3) | 0.0023(3) | 0.0065(2) |
| C3 | 0.2698(4) | −0.0081(5) | 0.7096(4) | 0.0061(3) | 0.0067(4) | 0.0057(4) | −0.0004(3) | 0.0011(3) | 0.0021(3) |
| C4A | 0.3672(6) | 0.0252(8) | 0.7706(7) | 3.74(16) | | | | | |
| C4B | 0.1487(8) | 0.0405(10) | 0.7826(9) | 3.17(19) | | | | | |
| C5 | 0.1119(4) | −0.0466(6) | 0.6408(5) | 0.0057(3) | 0.0122(7) | 0.0066(4) | −0.0020(4) | 0.0033(3) | 0.0027(4) |
| C6 | 0.1122(5) | −0.1026(6) | 0.5637(5) | 0.0080(4) | 0.0090(6) | 0.0055(4) | −0.0021(4) | 0.0024(3) | −0.0013(4) |
| C7 | 0.1902(6) | −0.1129(6) | 0.5596(5) | 0.0117(6) | 0.0087(6) | 0.0069(4) | 0.0029(5) | 0.0055(5) | 0.0001(4) |
| C8 | 0.2681(5) | −0.0670(7) | 0.6328(6) | 0.0073(4) | 0.0141(8) | 0.0088(6) | 0.0030(5) | 0.0053(4) | 0.0044(6) |
| N9A | 0.3852(5) | 0.1100(6) | 0.8274(5) | 3.39(12) | | | | | |
| N9B | 0.4070(7) | 0.2852(10) | 0.8596(7) | 3.66(18) | | | | | |
| C10 | 0.4839(4) | 0.1270(7) | 0.8933(4) | 0.0041(3) | 0.0168(9) | 0.0041(3) | −0.0014(4) | 0.0020(2) | 0.0021(4) |
| C11 | 0.4996(4) | 0.2392(7) | 0.9166(5) | 0.0047(3) | 0.0159(9) | 0.0055(4) | 0.0020(4) | 0.0033(3) | 0.0028(4) |
| C12A | 0.4463(7) | 0.3511(9) | 0.8882(7) | 4.04(17) | | | | | |
| C12B | 0.4139(9) | 0.0364(12) | 0.8250(10) | 3.78(22) | | | | | |
| C13 | 0.5537(7) | 0.0509(8) | 0.9317(6) | 0.0114(7) | 0.0148(9) | 0.0065(5) | 0.0030(7) | 0.0051(5) | 0.0041(5) |
| C14 | 0.6391(6) | 0.0858(12) | 0.9906(7) | 0.0059(5) | 0.0273(17) | 0.0095(7) | 0.0062(8) | 0.0039(5) | 0.0090(10) |
| C15 | 0.6568(5) | 0.1952(14) | 1.0174(6) | 0.0033(3) | 0.0326(19) | 0.0074(5) | −0.0032(7) | 0.0011(3) | 0.0039(10) |
| C16 | 0.5858(7) | 0.2744(8) | 0.9808(6) | 0.0099(6) | 0.0165(11) | 0.0074(5) | −0.0038(7) | 0.0043(5) | −0.0005(6) |
| N17A | 0.3603(5) | 0.3446(7) | 0.8540(5) | 3.62(13) | | | | | |
| N17B | 0.2455(6) | 0.3539(8) | 0.8580(7) | 3.30(17) | | | | | |
| C18 | 0.3149(7) | 0.4514(6) | 0.8070(6) | 0.0097(6) | 0.0070(6) | 0.0078(5) | 0.0017(5) | 0.0015(4) | −0.0020(4) |
| C19 | 0.2375(6) | 0.4608(6) | 0.8126(5) | 0.0082(5) | 0.0065(6) | 0.0074(5) | −0.0024(4) | 0.0018(4) | −0.0005(4) |
| C20A | 0.1922(6) | 0.3923(8) | 0.8634(7) | 3.61(15) | | | | | |
| C20B | 0.4100(10) | 0.3900(13) | 0.8368(11) | 4.49(26) | | | | | |
| C21 | 0.3365(6) | 0.5319(11) | 0.7586(8) | 0.0078(6) | 0.0186(13) | 0.0127(8) | 0.0008(7) | 0.0057(6) | −0.0028(9) |
| C22 | 0.2817(8) | 0.6254(8) | 0.7167(8) | 0.0130(8) | 0.0114(9) | 0.0156(10) | −0.0032(7) | 0.0100(8) | 0.0000(7) |
| C23 | 0.2050(7) | 0.6360(6) | 0.7245(7) | 0.0124(7) | 0.0072(6) | 0.0138(8) | 0.0025(5) | 0.0074(7) | 0.0021(6) |
| C24 | 0.1835(5) | 0.5524(8) | 0.7730(6) | 0.0071(4) | 0.0130(8) | 0.0100(6) | −0.0001(5) | 0.0043(4) | 0.0010(6) |
| N25A | 0.2097(5) | 0.2867(7) | 0.8786(5) | 3.47(12) | | | | | |
| N25B | 0.1909(6) | 0.1242(8) | 0.8409(6) | 2.93(15) | | | | | |
| C26 | 0.1754(4) | 0.2386(9) | 0.9382(5) | 0.0029(2) | 0.0218(11) | 0.0054(4) | −0.0004(4) | 0.0018(2) | 0.0032(5) |
| C27 | 0.1564(5) | 0.1258(8) | 0.9130(4) | 0.0054(3) | 0.0179(10) | 0.0046(3) | 0.0045(5) | 0.0024(3) | 0.0005(5) |
| C28A | 0.1527(6) | 0.0461(7) | 0.8320(6) | 3.21(14) | | | | | |
| C28B | 0.1995(8) | 0.3644(11) | 0.9054(9) | 3.42(21) | | | | | |
| C29 | 0.1626(5) | 0.2829(7) | 1.0129(5) | 0.0076(4) | 0.0119(8) | 0.0068(4) | −0.0031(5) | 0.0019(4) | −0.0018(5) |
| C30 | 0.1286(5) | 0.2165(7) | 1.0595(5) | 0.0067(4) | 0.0134(8) | 0.0062(4) | −0.0012(5) | 0.0040(3) | −0.0028(5) |
| C31 | 0.1095(5) | 0.1052(7) | 1.0342(5) | 0.0073(4) | 0.0134(8) | 0.0068(4) | −0.0015(5) | 0.0043(4) | 0.0001(5) |
| C32 | 0.1232(6) | 0.0605(7) | 0.9604(5) | 0.0107(6) | 0.0105(7) | 0.0056(4) | 0.0023(5) | 0.0028(4) | −0.0001(4) |
| B1 | 0.9655(5) | 0.2687(7) | 0.6901(6) | 4.95(14) | | | | | |
| F1A | 0.8787(4) | 0.2915(6) | 0.6227(4) | 6.45(14) | | | | | |
| F2A | 0.9750(5) | 0.2719(6) | 0.7827(5) | 8.68(17) | | | | | |
| F3A | 0.9842(5) | 0.1562(6) | 0.6838(5) | 8.05(17) | | | | | |
| F4A | 1.0222(6) | 0.3505(7) | 0.6909(6) | 9.87(20) | | | | | |
| F1B | 0.8730(9) | 0.2857(12) | 0.6556(10) | 3.85(24) | | | | | |
| F2B | 0.9736(18) | 0.3101(24) | 0.6070(20) | 11.06(67) | | | | | |
| F3B | 1.0102(13) | 0.3567(17) | 0.7546(15) | 7.28(40) | | | | | |
| F4B | 1.0094(9) | 0.1929(13) | 0.6660(10) | 4.41(25) | | | | | |

| | $x$ | $y$ | $z$ | $B$ |
|---|---|---|---|---|
| B2 | 0.4441(9) | 0.2199(12) | 0.6368(10) | 8.32(27) |
| F5A | 0.4423(10) | 0.1162(13) | 0.6271(11) | 18.21(47) |
| F6A | 0.3795(8) | 0.2579(12) | 0.6639(9) | 16.87(49) |
| F7A | 0.5159(6) | 0.2703(7) | 0.7132(6) | 11.10(21) |
| F8A | 0.4098(4) | 0.2815(6) | 0.5548(5) | 8.91(16) |
| F5B | 0.3719(17) | 0.1740(24) | 0.6470(19) | 7.65(57) |
| F6B | 0.4674(15) | 0.1229(20) | 0.5745(17) | 6.93(49) |
| F7B | 0.4665(17) | 0.1236(23) | 0.6931(20) | 7.46(56) |
| F8B | 0.5216(19) | 0.2642(24) | 0.6336(21) | 9.21(68) |

[a] In this table and those subsequent estimated standard deviations in the least significant figure are given in parentheses. Anisotropic thermal parameters are in the form $\exp[-(\beta_{11}h^2 + \beta_{22}k^2 + \beta_{33}l^2 + 2\beta_{12}hk + 2\beta_{13}hl + 2\beta_{23}kl)]$.

disordered fluorines. The Pd-$F_8$ distance is 2.95 (2) Å compared to the 3.1-3.2-Å sum of the van der Waals radii,[24] and the fluorine makes an angle of 90.6° with the $PdN_4$ planes. A close Ni-F approach of 2.70 Å was also observed in $[Ni(TAAB)][BF_4]_2$.[25]

The Pd-N bonds, averaging 2.004 (8) Å, are comparable to those observed in other complexes of palladium with macrocyclic systems. In tetraphenylporphinatopalladium(II) the Pd-N bonds average 2.009 Å,[26] while in the recently determined [5,7,12,14]tetramethyldibenzo[*b,i*][1,4,8,11]tetraaza[14]annulenepalladium(II) (PdTMTAA) a Pd-N distance of 1.996 Å was observed.[27] The three structural determinations for the TAAB ligand system reported to date illustrate the flexibility of the macrocycle to variations in metal-nitrogen bond lengths. A range of almost 0.2 Å is encountered from 1.90 (2) Å in $[Ni(TAAB)][BF_4]_2$[25] to 2.004 (8) Å in the analogous palladium complex to 2.09 (3) Å in the octahedrally coordinated $[Ni(TAAB)(I)(H_2O)][I]$.[25]

Within the cation the disorder lends some uncertainty to

**Table IV.** Final Positional and Thermal Parameters for Hydrogen Atoms in $[Pd(TAAB)][BF_4]_2$

| | $x$ | $y$ | $z$ | $B$ |
|---|---|---|---|---|
| HC5 | 0.050 | −0.040 | 0.640 | 6.0 |
| HC6 | 0.060 | −0.150 | 0.510 | 6.0 |
| HC7 | 0.195 | −0.160 | 0.510 | 6.8 |
| HC8 | 0.327 | −0.060 | 0.630 | 7.1 |
| HC13 | 0.552 | −0.030 | 0.900 | 7.6 |
| HC14 | 0.685 | 0.020 | 1.020 | 8.5 |
| HC15 | 0.715 | 0.230 | 1.060 | 8.3 |
| HC16 | 0.600 | 0.360 | 0.980 | 8.2 |
| HC21 | 0.400 | 0.530 | 0.757 | 8.8 |
| HC22 | 0.300 | 0.680 | 0.680 | 9.6 |
| HC23 | 0.150 | 0.690 | 0.680 | 9.5 |
| HC24 | 0.120 | 0.550 | 0.770 | 8.9 |
| HC29 | 0.170 | 0.370 | 1.030 | 7.7 |
| HC30 | 0.128 | 0.250 | 1.120 | 6.7 |
| HC31 | 0.090 | 0.061 | 1.070 | 7.2 |
| HC32 | 0.122 | 0.980 | 0.940 | 8.0 |

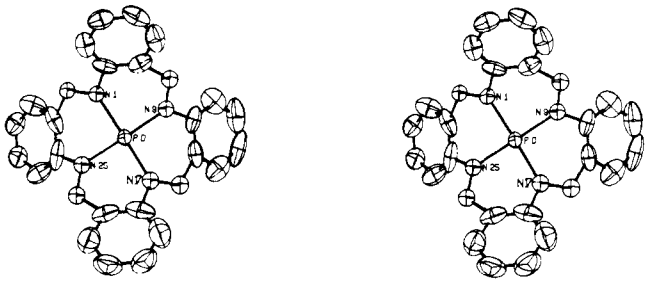

Figure 2. Stereoscopic view of $Pd(TAAB)^{2+}$ showing ellipsoids of 50% probability.

Table V. Hydrogen Atom Distances (Å)

| | | | |
|---|---|---|---|
| $HC_5$-$C_5$ | 1.05 | $HC_{24}$-$C_{24}$ | 1.09 |
| $HC_6$-$C_6$ | 1.04 | $HC_{25}$-$C_{25}$ | 1.00 |
| $HC_7$-$C_7$ | 0.98 | $HC_{26}$-$C_{26}$ | 1.06 |
| $HC_8$-$C_8$ | 1.02 | $HC_{27}$-$C_{27}$ | 1.05 |
| $HC_{13}$-$C_{13}$ | 1.06 | $HC_{29}$-$C_{29}$ | 1.05 |
| $HC_{14}$-$C_{14}$ | 1.03 | $HC_{30}$-$C_{30}$ | 1.02 |
| $HC_{15}$-$C_{15}$ | 0.97 | $HC_{31}$-$C_{31}$ | 0.93 |
| $HC_{16}$-$C_{16}$ | 1.04 | $HC_{32}C_{32}$ | 0.99 |

bond lengths and angles, especially for model B. The primary outcomes are several elongated C-C bonds and distorted inner ring angles compared to other TAAB systems.[25] Although the disordered portions of the macrocycle show the aforementioned deformities, which are undoubtedly artifacts of the disorder, the ordered benzo groups are well behaved and an average C-C length of 1.370 (11) Å and angles of 120.0 (8)° are observed. A comparison of the M-N and other appropriate bond lengths and angles is reported in Table IX for complexes of $M(TAAB)^{2+}$ where M is nickel and palladium.

The search for better models to account for disorder in the $BF_4$ anions was unsuccessful, leaving several unusual B-F distances and angles. The average bond lengths and angles for the anion, however, were 1.39 (2) Å and 106 (1)°, respectively, compared to an expected 1.43 (3) Å and 109.5°.[28]

In the recently reported PdTMTAA complex an interesting ring flattening effect, evidently related to the complexation of the palladium, is observed. Owing to steric interactions of the four methyl groups with the benzo rings the usual conformation for this ligand is highly saddle shaped.[29-31] In the palladium complex, however, the largest deviation of a macrocyclic nonhydrogen atom from the mean $N_4$ plane is only 0.467 Å, resulting in an almost planar geometry. In comparison, FeTMTAA has a maximum nonhydrogen displacement of 1.495 Å from the mean $N_4$ plane, associated with a carbon atom of one of the benzo groups.[29] Possible extended interactions of the larger d orbitals of palladium compared to first-row transition metals has been invoked to explain these observations.[27] Some evidence of ring flattening is also observed in $Pd(TAAB)^{2+}$, yet not nearly to the extent found for TMTAA complexes. In a comparison of $Pd(TAAB)^{2+}$ and the $Ni(TAAB)^{2+}$ analogue, the farthest displacements of a nonhydrogen macrocyclic atom from the mean $N_4$ plane are 2.93 Å for the former and 3.08 Å for the latter.[25] One possible explanation for the different effects of the metal ion is obtained in considering the nature of the distortion in the two ligand systems. For TMTAA the saddle-shaped distortion derives from steric interactions between the methyl and benzo groups. In the absence of the methyl groups the ligand system becomes planar.[32] The distortion in TAAB complexes can be related to steric interactions between benzo and methine hydrogens as well as inner ring bond angles. Whereas the size and strong coordinating abilities of the palladium can affect the steric interactions in TMTAA to the extent that planarity is approached, TAAB would appear to be less flexible with respect to metal-ion influence.

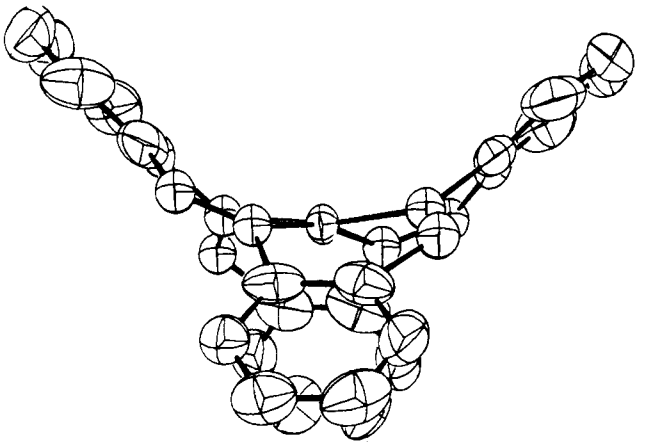

Figure 3. Perspective in-plane view of $Pd(TAAB)^{2+}$

Table VI. Interatomic Distances for $[Pd(TAAB)][BF_4]_2$ (Å)

| | | | |
|---|---|---|---|
| | A. Inner Ring Distances Model A | | |
| Pd-N1A | 2.034(7) | C11-C12A | 1.534(12) |
| Pd-N9A | 2.005(7) | C12A-N17A | 1.290(12) |
| Pd-N17A | 1.963(8) | N17A-C18 | 1.470(10) |
| Pd-N25A | 2.019(7) | C18-C19 | 1.356(11) |
| N1A-C2 | 1.442(5) | C19-C20A | 1.562(12) |
| C2-C3 | 1.401(9) | C20A-N25A | 1.272(12) |
| C3-C4A | 1.503(11) | N25A-C26 | 1.426(12) |
| C4A-N9A | 1.268(12) | C26-C27 | 1.378(11) |
| N9A-C10 | 1.492(9) | C27-C28A | 1.547(11) |
| C10-C11 | 1.360(10) | C28A-N1A | 1.289(11) |
| | B. Inner Ring Distances Model B | | |
| Pd-N1B | 1.992(10) | C12B-C10 | 1.566(15) |
| Pd-N9B | 2.046(10) | C11-N9B | 1.481(10) |
| Pd-N17B | 2.008(10) | N9B-C20B | 1.290(18) |
| Pd-N25B | 1.965(9) | C20B-C18 | 1.618(17) |
| N25B-C4B | 1.294(15) | C19-N17B | 1.416(12) |
| C4B-C2 | 1.594(13) | N17B-C28B | 1.310(15) |
| C3-N1B | 1.512(11) | C28B-C26 | 1.679(15) |
| N1B-C12B | 1.305(16) | C27-N25B | 1.496(11) |
| | C. Benzo Groups | | |
| C2-C5 | 1.373(9) | C18-C21 | 1.366(13) |
| C5-C6 | 1.370(9) | C21-C22 | 1.384(14) |
| C6-C7 | 1.358(10) | C22-C23 | 1.369(13) |
| C7-C8 | 1.370(11) | C23-C24 | 1.388(11) |
| C8-C3 | 1.368(10) | C24-C19 | 1.352(11) |
| C10-C13 | 1.368(11) | C26-C29 | 1.384(10) |
| C13-C14 | 1.348(14) | C29-C30 | 1.367(10) |
| C14-C15 | 1.340(16) | C30-C31 | 1.359(10) |
| C15-C16 | 1.405(15) | C31-C32 | 1.380(10) |
| C16-C11 | 1.375(11) | C32-C27 | 1.362(11) |
| | D. Anion | | |
| B1-F1A | 1.357(9) | B2-F5A | 1.228(17) |
| B1-F2A | 1.370(10) | B2-F6A | 1.420(16) |
| B1-F3A | 1.374(10) | B2-F7A | 1.358(14) |
| B1-F4A | 1.355(10) | B2-F8A | 1.333(13) |
| B1-F1B | 1.403(15) | B2-F5B | 1.413(28) |
| B1-F2B | 1.449(27) | B2-F6B | 1.664(27) |
| B1-F3B | 1.385(20) | B2-F7B | 1.367(28) |
| B1-F4B | 1.325(15) | B2-F8B | 1.436(29) |

Molecular packing is an important aspect of the structure in view of the interest in possible intermolecular interactions in this and the $I_3^-$ complexes. Owing to the extremely saddle-shaped geometry of the macrocyclic system, close intermolecular approach should be unfavorable and is indeed what is observed. The macrocyclic complexes stack in an almost

**Table VII.** Bond Angles (deg)

| | | | |
|---|---|---|---|
| | A. Inner Ring Model A | | |
| N1A-Pd-N9A | 90.1(3) | C12A-N17A-Pd | 125.2(7) |
| N9A-Pd-N17A | 91.8(3) | Pd-N17A-C18 | 121.9(6) |
| N17A-Pd-N25A | 90.8(3) | C12A-N17A-C18 | 111.7(8) |
| N25A-Pd-N1A | 89.2(3) | N17A-C18-C19 | 109.0(8) |
| Pd-N1A-C2 | 122.0(5) | N17A-C18-C21 | 130.4(8) |
| N1-C2-C3 | 107.5(6) | C18-C19-C20A | 135.4(8) |
| N1-C2-C5 | 133.0(6) | C24-C19-C20A | 104.7(7) |
| C2-C3-C4A | 138.1(7) | C19-C20A-N25A | 118.0(8) |
| C8-C3-C4A | 103.4(6) | C20A-N25A-Pd | 123.3(7) |
| C3-C4A-N9A | 117.9(8) | C20A-N25A-C26 | 112.1(8) |
| C4A-N9A-Pd | 124.5(7) | Pd-N25A-C26 | 124.0(6) |
| C4A-N9A-C10 | 113.4(8) | N25A-C26-C27 | 108.1(7) |
| Pd-N9A-C10 | 121.7(5) | N25A-C26-C29 | 132.5(8) |
| N9A-C10-C11 | 108.9(7) | C26-C27-C28A | 136.6(7) |
| N9A-C10-C13 | 131.0(7) | C32-C27-C28A | 103.7(7) |
| C10-C11-C12A | 138.0(7) | C27-C28A-N1A | 116.7(8) |
| C16-C11-C12A | 102.8(7) | C28A-N1A-Pd | 124.6(6) |
| C11-C12A-N17A | 117.3(8) | C28A-N1A-C2 | 112.0(7) |
| | B. Inner Ring Model B | | |
| N25B-Pd-N1B | 92.0(4) | C11-N9B-Pd | 124.7(7) |
| N1B-Pd-N9B | 89.8(4) | C11-N9B-C20B | 110.0(11) |
| N9B-Pd-N17B | 88.9(4) | Pd-N9B-C20B | 124.4(10) |
| N17B-Pd-N25B | 90.6(4) | N9B-C20B-C18 | 109.9(11) |
| Pd-N25B-C4B | 123.4(8) | N9B-C20B-C21 | 88.2(8) |
| N25B-C4B-C2 | 114.9(10) | C20B-C18-C19 | 151.2(9) |
| C4B-C2-C5 | 97.3(6) | C18-C19-N17B | 95.6(8) |
| C4B-C2-C3 | 143.2(7) | C24-C19-N17B | 144.6(8) |
| C2-C3-N1B | 99.7(6) | C19-N17B-Pd | 131.4(7) |
| C8-C3-N1B | 142.2(6) | C19-N17B-C28B | 104.9(10) |
| C3-N1B-Pd | 125.6(6) | Pd-N17B-C28B | 122.8(9) |
| C3-N1B-C12B | 108.2(10) | N17B-C28B-C29 | 94.9(7) |
| Pd-N1B-C12B | 124.7(9) | N17B-C28B-C26 | 112.7(10) |
| N1B-C12B-C10 | 113.3(11) | C28B-C26-C27 | 145.2(7) |
| C12B-C10-C13 | 93.6(7) | C26-C27-N25B | 95.9(7) |
| C12B-C10-C11 | 145.8(8) | C32-C27-N25B | 144.5(8) |
| C10-C11-N9B | 100.4(7) | C27-N25B-C4B | 104.5(9) |
| C16-C11-N9B | 140.4(6) | C27-N25B-Pd | 131.1(7) |
| | C. Benzo Groups | | |
| C2-C3-C8 | 118.0(6) | C18-C19-C24 | 119.7(7) |
| C3-C8-C7 | 122.1(7) | C19-C24-C23 | 120.9(8) |
| C8-C7-C6 | 119.6(6) | C24-C23-C22 | 119.5(8) |
| C7-C6-C5 | 119.8(6) | C23-C22-C21 | 118.6(8) |
| C6-C5-C2 | 121.1(6) | C22-C21-C18 | 121.0(8) |
| C5-C2-C3 | 119.3(5) | C21-C18-C19 | 120.2(8) |
| C10-C11-C16 | 119.2(7) | C26-C27-C32 | 119.4(6) |
| C11-C16-C15 | 119.7(9) | C27-C32-C31 | 121.0(7) |
| C16-C15-C14 | 119.4(8) | C32-C31-C30 | 119.7(7) |
| C15-C14-C13 | 120.6(9) | C31-C30-C29 | 119.9(6) |
| C14-C13-C10 | 120.9(10) | C30-C29-C26 | 120.5(7) |
| C13-C10-C11 | 120.1 (7) | C29-C26-C27 | 119.4(6) |
| | D. Anion | | |
| F1A-B1-F2A | 109.9(7) | F5A-B2-F6A | 112.0(14) |
| F1A-B1-F3A | 109.6(7) | F5A-B2-F7A | 120.1(14) |
| F1A-B1-F4A | 111.4(7) | F5A-B2-F8A | 116.4(14) |
| F2A-B1-F3A | 100.8(7) | F6A-B2-F7A | 95.6(11) |
| F2A-B1-F4A | 104.4(7) | F6A-B2-F8A | 94.1(10) |
| F3A-B1-F4A | 119.8(7) | F7A-B2-F8A | 113.2(11) |
| F1B-B1-F2B | 100.1(13) | F5B-B2-F6B | 105.4(17) |
| F1B-B1-F3B | 106.8(11) | F5B-B2-F7B | 66.1(16) |
| F1b-B1-F4B | 131.5(10) | F5B-B2-F8B | 175.7(19) |
| F2B-B1-F3B | 98.1(14) | F6B-B2-F7B | 74.4(16) |
| F2B-B1-F4B | 70.6(12) | F6B-B2-F8B | 75.6(15) |
| F3B-B1-F4B | 121.5(12) | F7B-B2-F8B | 110.4(18) |

zigzag arrangement along $z$ with Pd-Pd separations of 7.85 Å. The $BF_4^-$ anions are then situated in channels formed by the benzo groups along the $y$ axis. Because of extremely long Pd-Pd distances, intermolecular interactions in the $BF_4^-$ salt should be prohibited. Whether a significant decrease in metal-metal separations is possible in the $I_3^-$ complexes would seem unlikely in view of the results to be discussed in subsequent sections in which no changes in the electronic (and hence nonplanar) nature of the ligand system are indicated. Attempts to isolate single crystals of the $I_3^-$ suitable for X-ray analysis, the final proof of structure, are currently in progress.

**Table VIII.** Selected Least-Squares Planes and Atom Displacements (Å) for $[Pd(TAAB)][BF_4]_2$

| atom | distance | atom | distance |
|---|---|---|---|
| | A. Pd-N1A-N9A-N17A-N25A | | |
| | $-0.0445x + 0.2520y - 0.9667z = -10.4021$ | | |
| Pd | −0.0060 | N17A | 0.1887 |
| N1A | 0.1875 | N25A | −0.1861 |
| N9A | −0.1841 | | |
| | B. Pd-N1B-N9B-N17B-N25B | | |
| | $-0.0447x + 0.2147y - 0.9756z = -10.5746$ | | |
| Pd | −0.0248 | N17B | 0.1650 |
| N1B | 0.1633 | N25B | −0.1521 |
| N9B | −0.1515 | | |
| | C. C2-C3-C5-C6-C7-C8 | | |
| | $0.0520x + 0.8552y - 0.5157z = -5.1200$ | | |
| C2 | −0.0064 | C6 | 0.0057 |
| C3 | 0.0133 | C7 | 0.0014 |
| C5 | −0.0030 | C8 | −0.0110 |
| | D. C10-C11-C13-C14-C15-C16 | | |
| | $0.5999x + 0.1608y - 0.7838z = -8.4111$ | | |
| C10 | −0.0002 | C14 | 0.0192 |
| C11 | 0.0174 | C15 | −0.0017 |
| C13 | −0.0183 | C16 | −0.0164 |
| | E. C18-C19-C21-C22-C23-C24 | | |
| | $-0.1049x - 0.5030y - 0.8579z = -12.0165$ | | |
| C18 | −0.0100 | C22 | 0.0046 |
| C19 | 0.0102 | C23 | −0.0044 |
| C21 | 0.0025 | C24 | −0.0030 |
| | F. C26-C27-C29-C30-C31-C32 | | |
| | $-0.6920x + 0.2541y - 0.6757z = -5.1104$ | | |
| C26 | 0.0082 | C30 | 0.0052 |
| C27 | −0.0045 | C31 | −0.0015 |
| C29 | −0.0085 | C32 | 0.0012 |

**Table IX.** Interatomic Distances (Å) and Angles (deg)

| | [Ni(TAAB)-(I)($H_2O$)][I][a] | [Ni(TAAB)][$BF_4$]$_2$[a] | [Pd(TAAB)][$BF_4$]$_2$ |
|---|---|---|---|
| | Distances | | |
| M—N | 2.09(3) | 1.90(2) | 2.004(8)[c] |
| N—$C_{Ph}$ | 1.42(4) | 1.41(2) | 1.467(10) |
| $C_{Ph}$—$C_{Ph}$ | 1.40(2) | 1.33(4) | 1.370(11) |
| C—$C_{Ph}$ | 1.65[b] | 1.48(2) | 1.575(13) |
| C=N | 1.16[b] | 1.32(4) | 1.290(14) |
| | Angles | | |
| M—N=C | 130[b] | 123(2) | 124.2(8) |
| N=C—$C_{Ph}$ | 115[b] | 119(2) | 115.1(9) |
| C—$C_{Ph}$—$C_{Ph}$ | 135[b] | 130(3) | 141.7(8) |
| $C_{Ph}$—$C_{Ph}$—N | 113(3) | 113(3) | 103.1 (7) |
| $C_{Ph}$—N—M | 122(3) | 121(2) | 125.3(7) |
| $C_{Ph}$—$C_{Ph}$—$C_{Ph}$ | 120(4) | 120(2) | 120.0(7) |

[a] Reference 25. [b] These values were unreliable owing to disorder. [c] Esd's given are the mean of the esd's for parameters included in the average.

**Physical Measurements.** Major questions to be answered concern the formulation of iodine as well as the oxidation state of the $I_2$ reaction product. Has oxidation occurred, and if so, is it primarily ligand or metal ion centered? The following experiments were undertaken in order to answer these questions.

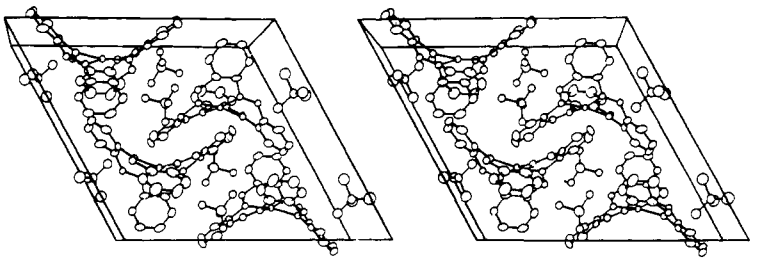

Figure 4. Packing diagram for $[Pd(TAAB)][BF_4]_2$ as viewed down the $y$ axis showing ellipsoids of 35% probability.

Table X. Binding Energies of Core Electrons for $[M(TAAB)]^{n+}$ Complexes (eV)

| | $3d_{3/2}$ | $3d_{5/2}$ | $4f_{5/2}$ | $4f_{7/2}$ |
|---|---|---|---|---|
| $[Pd(TAAB)][BF_4]_2$ | 343.74 | 338.49 | | |
| $[Pd(TAAB)][I_3]_{2.7}$ | 343.85 | 338.62 | | |
| $[Pt(TAAB)][BF_4]_2$ | | | 77.00 | 73.65 |
| $[Pt(TAAB)][I_3]_{2.7}$ | | | 76.93 | 73.62 |

Table XI. Conductivity Measurements for $M(TAAB)^{n+}$

| | conductivity, $\Omega^{-1}$ cm$^{-1}$ | | | |
|---|---|---|---|---|
| complex | single crystal | powder (1 bar) | powder (5 kbar) | powder (10 kbar) |
| $[Pd(TAAB)][BF_4]_2$ | | $1 \times 10^{-9}$ | $1 \times 10^{-8}$ | $8 \times 10^{-10}$ |
| $[Pd(TAAB)][I_3]_{2.7}$ | $10^{-7}$ | $5 \times 10^{-8}$ | $4 \times 10^{-6}$ | $5 \times 10^{-5}$ |
| $[Pt(TAAB)][BF_4]_2$ | | $1 \times 10^{-9}$ | $1 \times 10^{-7}$ | $2 \times 10^{-7}$ |
| $[Pt(TAAB)][I_3]_{2.7}$ | $10^{-4}$ | $6 \times 10^{-7}$ | $6 \times 10^{-6}$ | $6 \times 10^{-6}$ |

The mid-infrared spectra of the $I_3^-$ complexes are virtually superimposable on those of the corresponding $BF_4^-$ compounds, indicating that the ligand system remains unchanged upon reaction with $I_2$. With the exception of several enhanced intensities there is no noticeable change in the spectra up to 20 kbar pressure. The infrared absorption spectra have previously been assigned by Busch and co-workers.[33] The far-infrared region is especially diagnostic for $I_3^-$ absorptions. Theory predicts two bands to be infrared active for the linear $I_3^-$ ion.[34] One is the asymmetric stretching mode, $\nu_3$, observed at 135 cm$^{-1}$ for both the palladium and platinum complexes. The other, the doubly degenerate bending mode, $\nu_2$, is seen weakly at 42 cm$^{-1}$ for the palladium and 46 cm$^{-1}$ for the platinum complex. A weak band at 104 cm$^{-1}$, possibly assignable to the totally symmetric stretch, $\nu_1$, is also observed. Infrared activity for this mode suggests some dissymmetry in the I-I-I bonds ($C_{\infty_h}$ symmetry). The totally symmetric Raman-active stretch, $\nu_1$, was observed at 109 cm$^{-1}$ for the palladium complex using both 514.5- and 488.0-nm excitation. The platinum analogue, however, decomposed in the laser beam so that the symmetric stretch could not be observed. No evidence of $I_2$ was observed in the 210-180-cm$^{-1}$ region in the Raman spectra for the palladium complex.[35]

Magnetic susceptibility measurements for both $I_3^-$ complexes using the Faraday method showed no evidence of paramagnetism. ESR is a particularly suitable method for examining the question of metal-centered or ligand-centered hole states. The ESR spectra of the $I_2$ oxidation products of 1,4,5,8,9,12,13,16-octamethyltetrabenzporphinatonickel(II), for example, consist of a single line ($W_{pp} \sim 5$ G) with $g_\parallel = 2.012$ located along the direction of stacking and $g_\perp = 2.006$, which indicates $\pi$ cation radical or largely macrocycle associated hole states.[9,10] The partially oxidized tetracyanoplatinates, on the other hand, reveal ESR signals characteristic of $d_{z^2}$-like hole states. Oriented single crystals of $K_2Pt(CN)_4(Br_{0.30})(H_2O)_3$, for example, exhibit temperature-independent values of $g_\parallel = 1.946$ (5) and $g_\perp = 2.336$ (5).[36] The ESR spectra of crystalline samples of the $I_2$ reaction products of $M(TAAB)^{2+}$ did show broad, weak signals centered at $g = 2.1$ for both the palladium and platinum complexes. In a search for a paramagnetic impurity which might be responsible for the ESR signal both the $I_2$ used in the reactions and the $[M(TAAB)][BF_4]_2$ complexes were examined. Neither the $I_2$ nor the $[Pd(TAAB)][BF_4]_2$ showed any evidence of paramagnetism; however, the $[Pt(TAAB)][BF_4]_2$ showed an extremely weak signal in the same position as that of the $I_3^-$ derivative. The question of the degree of oxidation and in fact whether oxidation has actually occurred thus remains open. From both mid-infrared and EPR data, however, it can be concluded that the TAAB complexes do not mimic the behavior of the phthalocyanines and tetrabenzporphyrins in a primarily ligand-centered oxidation.[9,10]

The X-ray photoelectron spectra of both the $I_3^-$ and $BF_4^-$ salts were examined in order to determine the presence of an oxidation state greater than 2+. The results are tabulated in Table X. As can be seen by examining the $3d_{3/2}$ and $3d_{5/2}$ binding energies for palladium and the $4f_{5/2}$ and $4f_{7/2}$ binding energies for platinum, no shifts to higher energies, which would be indicative of a higher oxidation state for the metal, are observed. The ratios of band heights, another measure of the integrity of the oxidation state, also indicate a 2+ state for the metal ions. Analyses of samples which had been subjected to vacuum for over 24 h showed no decrease in I content, although possible decomposition of the complex under X-ray PES conditions could still be a factor in view of similar findings for certain partially oxidized tetracyanoplatinates.[37]

The room temperature conductivity data are reported in Table XI. Single-crystal measurements for the $I_3^-$ samples show the anticipated trend for primarily metal-centered interactions: an increase of $10^3$ for the platinum compared to the palladium complex. This effect is thought to be due to the greater spatial extension of the 5d compared to the 4d orbitals.[1] Also as expected, the $I_3^-$ complexes exhibit a conductivity greater than that of $BF_4^-$ salts. Other partially oxidized bisdioximates have shown somewhat greater increases over their unoxidized counterparts, however, of $10^3$-$10^4$ $\Omega^{-1}$ cm$^{-1}$,[1] compared to $10^2$ for the TAAB complexes. An interesting effect of pressure on the pressed powder conductivity is observed. Increases in conductivity of up to $10^3$ are observed for the $[Pd(TAAB)][I_3]_{2.7}$ for pressures up to 10 kbar. The effect is apparently less for the platinum analogue. Neither mid-infrared nor visible absorption spectra show discernible changes at up to 20 kbar pressure. The lack of spectral changes in these regions indicates that neither gross intramolecular changes in the ligand system nor phase changes are occurring. Hence, the pressure effects could be related to decreases in intermolecular separations resulting in increased interactions.

Two aspects of these complexes are unique with respect to previously studied macrocyclic systems: the sterically hindered saddle-shaped ligand system and the large iodine content (greater than 60% by weight). The partially oxidized bisdioximates, which exhibit conductivities on the same order of magnitude as the $I_2$ reaction products of TAAB, are consid-

erably more planar and possess intermolecular separations on the order of 3.2 Å. Although the degree of oxidation of the TAAB complexes remains in question, these complexes do show larger than expected conductivities (especially when compared with the bisdioximates) along with an unusual pressure dependence, perhaps related to compression of the unit cell. Possible influences of the large percentage of iodine on the conductivity are currently being investigated in related systems with high iodine content.

**Acknowledgments.** The authors wish to thank Drs. R. J. Thorn, J. McCreary, L. J. Basile and P. LaBonville Walling for their research contributions and helpful discussions during the course of this work. K.B.M. acknowledges the donors of the Petroleum Research Fund, administered by the American Chemical Society, and the University of Kansas General Research allocation no. 3227-X0-0038 for support of this research.

**Supplementary Material Available:** Table II, observed and calculated structure factors for $[Pd(TAAB)][BF_4]_2$ (37 pages). Ordering information is given on any current masthead page.

## References and Notes

(1) (a) This work was performed under the auspices of the Division of Basic Energy Sciences of the U.S. Department of Energy. (b) University of Kansas. (c) Argonne National Laboratory.
(2) (a) Miller, J. S.; Epstein, A. J. *Prog. Inorg. Chem.* **1976**, *20*, 1–151, and references cited therein. (b) Thomas, T. W.; Underhill, A. E. *Chem. Soc. Rev.* **1972**, *1*, 99–120.
(3) Endres, H.; Keller, H. J.; Lehmann, R. *Inorg. Nucl. Chem. Lett.* **1975**, *11*, 769–771.
(4) Endres, H.; Keller, H. J.; Megnamisi-Bélombé, M.; Nöthe, D. *Z. Naturforsch. B* **1975**, *30*, 535–538.
(5) Gleizes, A.; Marks, T. J.; Ibers, J. A. *J. Am. Chem. Soc.* **1975**, *97*, 3545–3546.
(6) Miller, J. S.; Goldberg, S. Z. *Inorg. Chem.* **1975**, *14*, 2294–2296.
(7) Miller, J. S.; Griffiths, C. H. *J. Am. Chem. Soc.* **1977**, *99*, 749–755.
(8) Petersen, J. L.; Schramm, C. S.; Stojakovic, D. R.; Hoffman, B. M.; Marks, T. J. *J. Am. Chem. Soc.* **1977**, *99*, 286–288.
(9) Schramm, C.; Stojakovic, D. R.; Hoffman, B. M.; Marks, T. J. *Science* **1978**, *200*, 47–48.
(10) Phillips, T. E.; Hoffman, B. M. *J. Am. Chem. Soc.* **1977**, *99*, 7734–7736.
(11) Miller, J. S. *Inorg. Chem.* **1976**, *15*, 2357–2360.
(12) Mertes, K. B.; Ferraro, J. R. *J. Chem. Phys.* **1979**, *70*, 646–648.
(13) Basile, L. J.; Ferraro, J. R., unpublished data.
(14) Ferraro, J. R.; Basile, L. J. *Appl. Spectrosc.* **1974**, *28*, 505–516.
(15) Walling, P.; Ferraro, J. R. *Rev. Sci. Instrum.* **1978**, *49*, 1557–1558.
(16) Varian "EPR at Work" series, No. 28.
(17) Brawner, S.; Mertes, K. B. *J. Inorg. Nucl. Chem.*, **1979**, *41*, 764–767.
(18) Computer programs for unit cell calculation and collection of data were supplied by Syntex Analytical Instruments.
(19) Mertes, K. B., *Inorg. Chem.* **1978**, *17*, 49–52.
(20) The programs used were local modifications of A. Zalkin's FORDAP for the Fourier summation, W. Busing, K. Martin, and H. Levy's ORFLS and ORFFE-II for least-squares and function and error calculations, and C. K. Johnson's ORTEP-II for the molecular structure drawing. Computations were performed on the Honeywell 66/60 computer at the University of Kansas.
(21) Thomas, L. H.; Umeda, K. *J. Chem. Phys.* **1957**, *26*, 293–303.
(22) Cromer, D. T.; Mann, J. B. *Acta Crystallogr., Sect. A* **1968**, *24*, 321–324.
(23) Ibers, J. A. "International Tables for X-ray Crystallography", Vol. III; Kynoch Press: Birmingham, England, 1968; Tables 3.3.1A and 3.3.2C.
(24) Bondi, A. *J. Phys. Chem.* **1964**, *68*, 441–457.
(25) Hawkinson, S. W.; Fleischer, E. B. *Inorg. Chem.* **1969**, *11*, 2402–2410.
(26) Fleischer, E. B.; Miller, C. K.; Webb, L. E. *J. Am. Chem. Soc.* **1964**, *86*, 2342–2347.
(27) Tsutsui, M.; Bobsein, R. L.; Cash, G.; Pettersen, R. *Inorg. Chem.* **1979**, *18*, 758–761.
(28) Oendik, H.; Smith, D. In ref 23, Table 4.4.1.
(29) Goedken, V. L.; Pluth, J. J.; Peng, S.-M.; Bursten, B. J. *J. Am. Chem. Soc.* **1976**, *98*, 8014–8021.
(30) Weiss, M. C.; Bursten, B.; Peng, S.-M.; Goedkin, V. L. *J. Am. Chem. Soc.* **1976**, *98*, 8021–8031.
(31) Weiss, M. C.; Goedken, V. L. *Inorg. Chem.* **1979**, *18*, 274–279.
(32) Weiss, M. C.; Gordon, G.; Goedken, V. L. *Inorg. Chem.* **1977**, *16*, 305–310.
(33) Melson, G. A.; Busch, D. H. *J. Am. Chem. Soc.* **1964**, *86*, 4384–4387.
(34) Gabes, W.; Gerding, H. *J. Mol. Struct.* **1972**, *14*, 267–279.
(35) Kiefer, W. *Appl. Spectrosc.* **1974**, *28*, 115–133.
(36) Mehran, F.; Scott, B. A. *Phys. Rev. Lett.* **1973**, *31*, 1347–1349.
(37) Thorn, R. J., private communication.

# Novel Organosilicon Radical Cations. One-Electron Oxidation of Permethylcyclopolysilanes[1]

**H. Bock,[2a] W. Kaim,[2a] M. Kira,[2a] and R. West*[2b]**

*Contribution from the Chemistry Departments, University of Frankfurt, Theodor-Stern-Kai 7, D-6000 Frankfurt/Main, West Germany, and the University of Wisconsin, Madison, Wisconsin 53706.* *Received November 27, 1978*

**Abstract:** The permethylcyclosilanes **1**–**4**, all of which exhibit low first ionization potentials, have been oxidized with $AlCl_3$ in $CH_2Cl_2$ to form the first examples of delocalized, $\sigma$-electron radical cations. These species have been studied by ESR spectroscopy. Unlike the well-known radical anion of **1**, the radical cation of dodecamethylcyclohexasilane ($\mathbf{1}^{+\cdot}$) gives an ESR spectrum which can be simulated only by assuming two sets of 18 equivalent protons, corresponding to 6 axial and 6 equatorial methyl groups which do not become equivalent on the ESR time scale. The high $g$ value of 2.0093 observed for $\mathbf{1}^{+\cdot}$ suggests a considerable spin population in the $Si_6$ ring skeleton. The radical cations of **2**, **3**, and **4** show only overlapping signals in ESR, but their respective $g$ values of 2.010, 2.0105, and 2.0063 are also consistent with spin delocalization into the $\sigma_{Si-Si}$ system.

Peralkylpolysilanes have attracted interest because of their unique properties which distinguish these compounds from saturated catenates of carbon.[3] In particular, cyclic polysilanes resemble in their behavior aromatic hydrocarbons, in that they show long-wavelength ultraviolet absorption,[4] undergo one-electron reduction to radical anions,[5] form charge-transfer complexes with $\pi$ acceptors,[6] and have low first ionization potentials.[7] Because the latter are similar to those of aromatic compounds like naphthalene and anthracene,[8] several attempts have been made to oxidize polysilanes to cation radicals.[9]

Recently, organosilicon compounds containing lone electron pairs or $\pi$-electron systems have been oxidized to persistent[10] radical cations in a straightforward way using the system $AlCl_3/CH_2Cl_2$. The redox potential of this mixture is sufficient to oxidize compounds which have a first (adiabatic) ionization potential below 8 eV. Examples containing silicon are shown in Chart I. Although permethylcyclopolysilanes contain neither $\pi$ electrons nor lone pairs, the rather small effective nuclear charge of silicon leads to low (<8 eV) ionization potentials for Si–Si $\sigma$-bonding electrons. We find that compounds **1**–**4** (R = $CH_3$) can be oxidized by $AlCl_3/CH_2Cl_2$ at low temperatures

0002-7863/79/1501-7667$01.00/0 